Brackish springs in coastal aquifers and the role of calcite dissolution by mixing waters

Esteban Sanz Escudé

October 19, 2007

CHAPTER 4: REACTIVE TRANSPORT MODELLING OF S'ALMADRAVA BRACKISH SPRING

PhD Thesis
Department of Geotechnical Engineering and Geo-Sciences (ETCG)
Technical University of Catalonia (UPC)

Supervisors:
Dr. Jesús Carrera Ramírez
Dr. Carlos Ayora Ibáñez

Institute of Earth Sciences 'Jaume Almera', CSIC

Chapter 4

Reactive transport modelling of S'Almadrava brackish spring

On Chapter 3 of this thesis we proposed a hypothetical, but geologically feasible, dual permeability conceptual model to explain the hydrogeological behaviour of S'Almadrava spring (8 m.a.s.l., Mallorca, Spain). Briefly, it assumes that mixed waters flow up from a conduit branching (at an estimated location of -540 m.a.s.l.) towards the spring mouth through two different media: a well developed karst conduit with fast turbulent flow and an intensely fractured matrix with low Darcyan flow. Flow and transport simulations confirmed that this conceptual model was able to explain both the main pattern of increasing concentration with a decrease in the spring discharge, and the two main peculiarities of the spring: double high salinity peak at the end of the dry season and a secondary salinity peaks in the middle of the sudden salinity drop when a new rainfall event is produced. However, despite of the good performance of the numerical model, the limited geological information at depth impeded the ultimate validation of the conceptual model. Thus, a complementary validation of the dual permeability conceptual model is proposed based on the interpretation of high-frequency geochemical data collected in the spring. The reason for using geochemistry is that the composition of the water being discharged in the spring is the immediate result of the water-rock interaction processes occurring in those deep non-accessible carbonate systems.

The use of geochemical data is not common in studies on brackish springs and traditionally only salinity (or chloride concentration) measurements are available. This may be due to several factors including the believe that geochemistry of the system is essentially that of a simple mixture of freshwater and seawater, the difficulties that may arise when designing an appropriate sampling campaign in these highly dynamic systems, or the notable higher cost of obtaining geochemical data with respect to salinity measurements. Most of previous geochemical studies are devoted to the identification of the salinity sources and recharge areas in the aquifer by means of Cl/Br ratios or the δ^2H, δ^{18}O of the water molecule (Payne et al., 1978; Leontiadis et al., 1988; Blavoux et al., 2004; Arfib et al., 2007). More specifically for S'Almadrava spring (Appendix A) used the analysis of δ^{34}S and δ^{18}O of dissolved sulfate to identify the salinity sources in the spring. They concluded that the effect of salinity sources other than seawater (like the dissolution of evaporites dissolution from the Keuper strata or contamination by fertilizers), was practically negligible at any stage of the spring functioning. But besides the identification of the salinity sources, the detailed temporal evolution of the geochemistry in the spring is still not well characterized. In fact, these highly dynamic systems need an evaluation of their temporal evolution for a complete characterization.

The objectives of this study are to interpret high-frequency geochemical data obtained from S'Almadrava brackish spring during a field campaign on November-December 2004, and to build a reactive transport model in order to unravel the water-rock interaction processes that take place at depth. Up to our knowledge, this is the first time that reactive transport modelling is used for the quantitative assessment of geochemical processes in such a flow-complex system. Ultimately, the reactive transport modelling may allow a further validation of the dual permeability conceptual model for S'Almadrava spring.

4.1. Geochemical data

4.1.1. Geochemical sampling

Most of the brackish springs present a roughly cyclic behaviour strongly dependent on the recharge regime. A monitoring program for brackish springs must incorporate a flow-dependent, high frequency sampling strategy along with the traditional long-term low-frequency sampling. Ryan and Meiman (1996) successfully applied this methodology for examining the short-term variations of water quality in freshwater karst springs of Kentucky. Therefore, the general functioning of these systems could be identified by means of a long-term monitoring of the spring salinity and discharge (for example with an automatic probe and flow meter at the spring mouth or regular measurement of the discharge) (Sanz et al., 2002; Fleury et al., 2007b). This long-term monitoring also allowed the identification of the cyclic patterns of the spring, thus favouring the design of a high frequency sampling for geochemistry during the minimum time

period being repeated (e.g., one or two spring cycles). The situations showing the sharpest changes in salinity or temperature deserved a special attention for a detail characterization of the quality variation of the spring discharge.

A considerable amount of historical data is available for S'Almadrava spring, with daily measurements of rainfall at the recharge area and discharge flow, and hourly measurements of electric conductivity (EC) and temperature at the spring discharge, discontinuously for the last 10 years. This has permitted a complete characterization of the spring salinity with the spring discharge (recall Chapter 3). The spring describes well defined cycles (spring cycle) of similar time duration between consecutive rainfall events. When a new rainfall produces, the spring salinity drops sharply to begin to increase gradually with the decrease of the runoff until a new rainfall event occurs. In the middle of the salinity drop following a rainfall event, a secondary salinity peak is produced (secondary peak). Another peculiarity is the double high salinity peak (high peak) observed when the spring reactivates after a long dry period. This pattern has been observed with little variations for many years and was used to design the high-frequency sampling campaign focusing on the reactivation of the spring after a dry period and the following spring cycle.

The sampling campaign was carried out during the spring reactivation after the long dry summer of 2004. Samples were taken during a period of approximately 40 days covering 2 rainfall events (Figure 4.1). During that period samples were collected using an automatic ISCO Model 6712 water sampler located at the spring mouth. The sampler was installed during the summer when the spring was dried-up, and was programmed to draw a sample from the spring at 1 to 8-hour intervals, after the first spring reactivation. During this period, up 110 samples of 1000 mL were collected. Additionally, electric conductivity was measured manually at the spring mouth approximately once a week from July 2004 to certify that no unexpected salinity variations were produced at the spring mouth before the sampling program began. Rainfall distribution, flow discharge evolution and electric conductivity measured in the samples are shown in Figure 4.1.

Full sampling bottles were replaced with empty bottles every day and stored at low temperature after measuring the pH and Electrical Conductivity (EC). The differences between the pH measured directly at the spring mouth with that in the bottles allows to recalculate alkalinity and CO_2 degassing in the sample bottles. Figure 4.2 shows unambiguously that the sampling period covered a peak of high salinity after the spring reactivation (a to c, Figure 4.2), a full spring cycle between two consecutive rainfall events (c to d, Figure 4.2), and a secondary salinity peak in the middle of the salinity drop (e, Figure 4.2), which are the key features of the spring. It should be noted that the beginning of the sampling period only covered the second of the double high salinity peak after the summer. The formation of this double high salinity peak has been observed repeatedly over the years (recall Chapter 3) and therefore is likely to occur

also after the summer of 2004. The fact that the field measurements only show one peak is attributed to a late activation of the sampling program in the autosampler. It should be noted that because of the sharp EC (and presumably water chemistry) changes occurring in the spring, these variations can only be described with few-hour sampling intervals. Based on the EC variation curve among the 110 samples, we selected 23 samples for pH, alkalinity and major ions concentration measurements at the laboratory (Figure 4.2). Electric conductivity was measured with a MYRON L company 6P Ultrameter, pH with a ThermoORION 9157BN electrode and alkalinity by titration. Analysis for Na, K, Ca, Mg, Sr and S were made by ICP while analyses for Cl were made by HPLC. Local seawater at the Pollença bay was also sampled (at 0 m.a.s.l.) and analyzed to complete the characterization of the system. Analytical errors were 5%, 0.02 pH units, 3% and 5% for EC, pH, ICP and HPLC measurements, respectively.

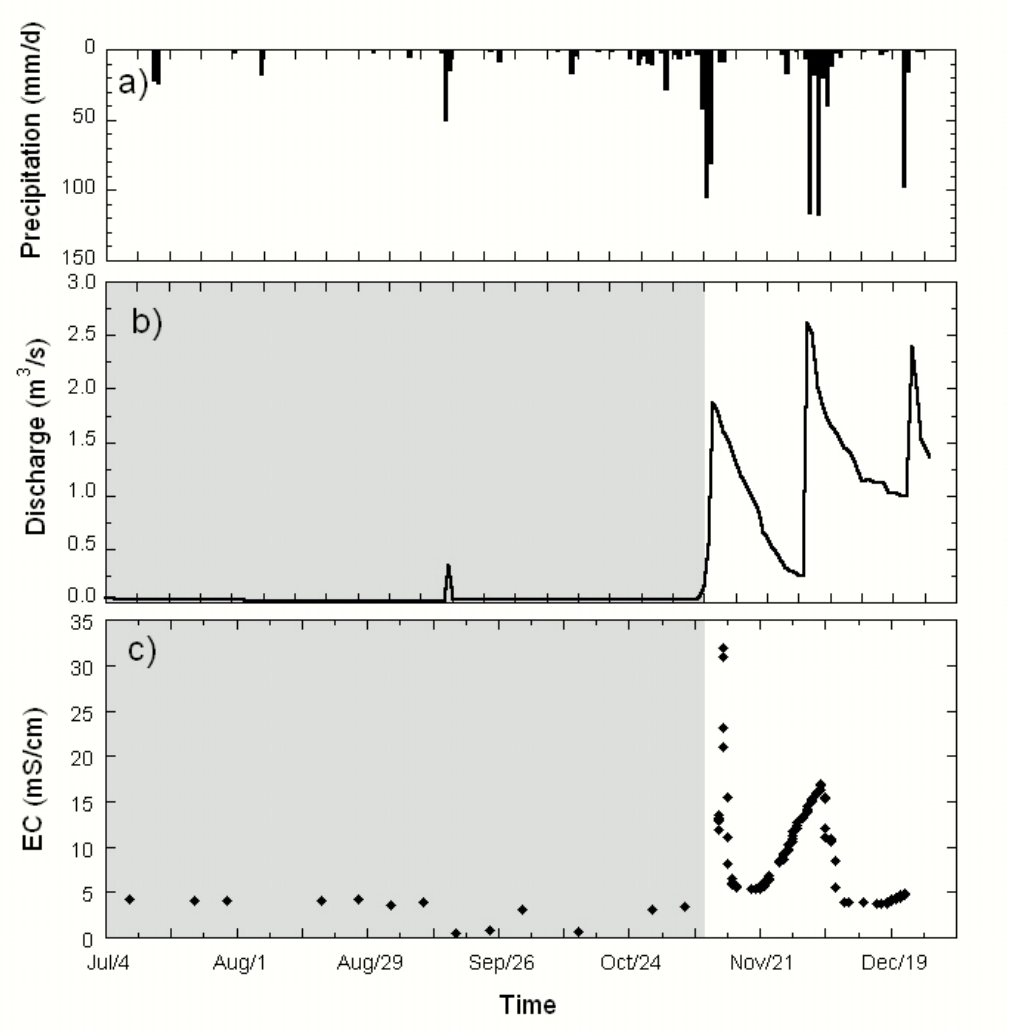

Figure 4.1: Field measurements of rainfall at the recharge area, spring flow discharge and electrical conductivity (EC) of S'Almadrava spring, during the period July-December 2004. Grey area shows the period when the spring is dry.

4.1.2. Chemical results

Analysis results obtained in S'Almadrava spring during the sampling period are listed in Table 4.1, Figure 4.3 and Figure 4.4 show the results for major ions with respect to the chloride content. The chloride concentration is assumed to be conservative in the system. Similarly to Figure 4.2, samples are grouped depending on the spring stage they represent, that is, the spring cycle between consecutive rainfall events, the high salinity peak after spring reactivation, and secondary salinity peak in the middle of the salinity drop. The time variation of the water chemistry discharging in S'Almadrava spring is discussed in Figure 4.3 with the results for Calcium. Note that the letters in this figure are consistent with those on Figure 4.2. When the spring reactivates after a long dry period, the Ca concentration increases sharply with Cl (or total salinity) (a to b, Figure 4.3) and then decreases again to the lowest concentration measured in the spring (b to c, Figure 4.3). The relation of Ca/Cl on samples of the high salinity peak is much higher than the one expected from a conservative mixing with seawater (dashed line, Figure 4.3).

After the high salinity peak ends, the spring initiates a spring cycle with a gradual increase of salinity with the reduction of spring discharge (Figure 4.1). During this period concentration of Ca increase (c to d, Figure 4.3) proportional to that of Cl and follows a different pattern than that during the high salinity peak. In fact, samples align close to the conservative mixing, except for the more saline waters (d, Figure 4.3). Following the time evolution, when a new rainfall event occurs and the secondary salinity peak develops (d to e, Figure 4.3), the ratio Ca/Cl increases compared to the group of samples during spring cycle. This higher Ca/Cl ratio is similar to the one observed during the high salinity peak. Finally, after the secondary salinity peak, the water salinity continues reducing (e to c, Figure 4.3) and a new spring cycle begins (c to d, Figure 4.3). It is clear that the set of results do not describe a single mixing line between two end-members, but rather distinct a geochemical signals for every group of samples. Therefore, some water-rock reactions are expected to occur in addition to conservative mixing.

A geochemical pattern similar to that observed for Ca is also distinguished for the rest of major cations, except for Na (Figure 4.4). Thus, samples from the high salinity peak show an excess of Sr and a depletion of Mg and K, with respect to the samples collected during the spring cycle. And the chemistry of the samples collected during the secondary salinity peak also appears to be similar to that of the high salinity peak. It should be noted that the samples from the spring cycle do not align exactly with the conservative mixing line. On the other hand, Na results for any stage of the spring functioning apparently align in one single line very similar to the conservative mixing drawn in Figure 4.4.

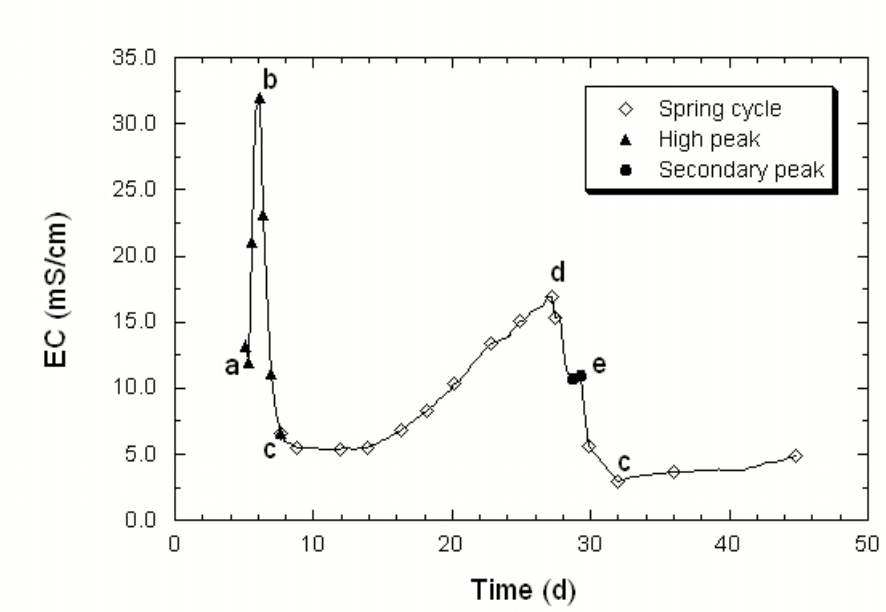

Figure 4.2: Field measurement of electrical conductivity (EC) variation of S'Almadrava spring, based on all samples collected during the period of November-December 2004 (line). Samples selected for major ions analysis are also indicated, using different symbols depending on the spring stage they represent: spring cycle, high salinity peak after summer (high peak) and the secondary salinity peak in the middle of the salinity drop (secondary peak). The meaning of the letters is discussed in the text.

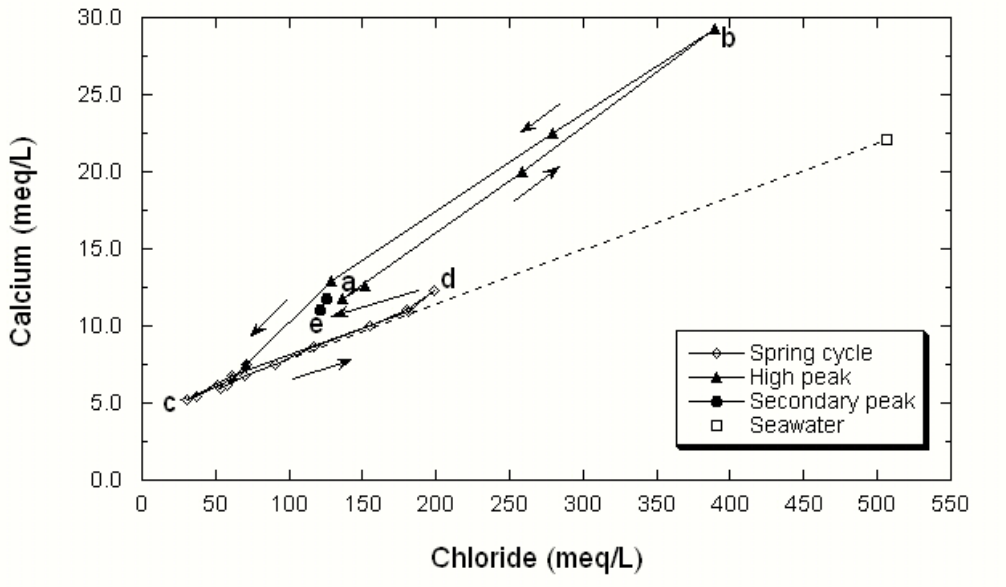

Figure 4.3: Relationship of calcium with chloride content, for the sampling period of November-December 2004. The time sequence of the sampling is marked with arrows. Letters indicate particular stages of the spring discussed in the text. Analyses are grouped as the spring feature they represent: spring cycle, high salinity peak after summer (high peak) and secondary salinity peak (secondary peak). Dashed line represents the conservative mixing between the fresher water sampled in the spring and the local seawater (M-21 and Local sea in Table 4.1, respectively).

Sample code	Date mm/dd/yy hh:mm	EC mS/cm	pH field	Alkalinity ppm $CaCO_3$	Cl meq/L	Na meq/L	K meq/L	Ca meq/L	Mg meq/L	Sr meq/L	S meq/L
M-1	11/12/04 14:10	17.100	8.30	236.4	151.89	133.00	3.29	12.62	27.22	0.060	9.03
M-2	11/12/04 22:10	15.430	8.35	183.4	136.82	118.65	3.00	11.73	24.87	0.055	8.16
M-3	11/13/04 02:10	27.400	8.20	139.9	258.99	226.86	5.68	20.02	45.38	0.100	15.38
M-4	11/13/04 16:10	41.530	8.32	168.9	389.58	361.05	8.60	29.23	68.51	0.148	24.54
M-5	11/13/04 23:10	30.110	8.37	164.1	279.24	255.33	6.18	22.55	49.32	0.108	17.04
M-6	11/14/04 13:10	14.450	8.49	207.5	128.29	113.89	2.70	12.96	22.42	0.058	7.86
M-7	11/15/04 03:10	8.521	8.59	135.1	70.99	61.69	1.58	7.48	13.82	0.031	4.31
M-8	11/16/04 07:10	7.201	8.36	231.6	61.26	49.49	1.30	6.57	11.87	0.025	3.59
M-9	11/19/04 11:30	7.034	8.45	188.2	58.03	48.68	1.28	6.12	10.99	0.023	3.37
M-10	11/21/04 11:30	7.182	8.46	120.6	53.92	51.11	1.30	5.90	11.68	0.023	3.57
M-11	11/23/04 19:30	8.859	8.47	197.8	70.11	66.85	1.70	6.76	14.97	0.029	4.64
M-12	11/25/04 16:52	10.820	8.32	197.8	90.81	79.54	2.10	7.50	17.86	0.035	5.49
M-13	11/27/04 17:52	13.380	8.23	193.0	116.88	102.02	2.68	8.64	22.41	0.043	6.97
M-14	11/30/04 08:52	17.390	8.00	193.0	154.78	137.25	3.62	9.97	29.90	0.056	9.39
M-15	12/02/04 09:52	19.550	7.83	189.1	180.15	156.19	4.09	11.02	33.53	0.063	10.60
M-16	12/04/04 17:52	22.050	8.11	188.2	198.19	178.40	4.68	12.26	38.16	0.072	12.13
M-17	12/05/04 00:52	19.960	8.10	169.8	181.40	160.78	4.25	10.91	34.09	0.064	10.91
M-18	12/06/04 04:52	13.860	8.20	177.6	121.00	104.32	2.63	11.09	21.33	0.049	7.18
M-19	12/06/04 18:52	14.270	8.44	197.8	125.17	110.11	2.73	11.78	21.78	0.051	7.62
M-20	12/07/04 08:52	7.258	8.53	204.6	61.33	51.00	1.33	6.82	11.49	0.026	3.60
M-21	12/09/04 11:00	3.842	8.30	222.0	30.11	24.01	0.62	5.20	6.13	0.014	1.88
M-22	12/13/04 12:30	4.780	8.42	204.6	37.66	30.32	0.80	5.42	7.28	0.015	2.25
M-23	12/22/04 07:50	6.322	8.25	212.3	51.46	42.49	1.11	6.16	9.88	0.021	3.04
Local sea	November 2004	53.650	7.95	127.4	506.15	459.16	11.42	22.05	103.44	0.176	31.17

Table 4.1: Analysis results of samples of S'Almadrava spring used in this study

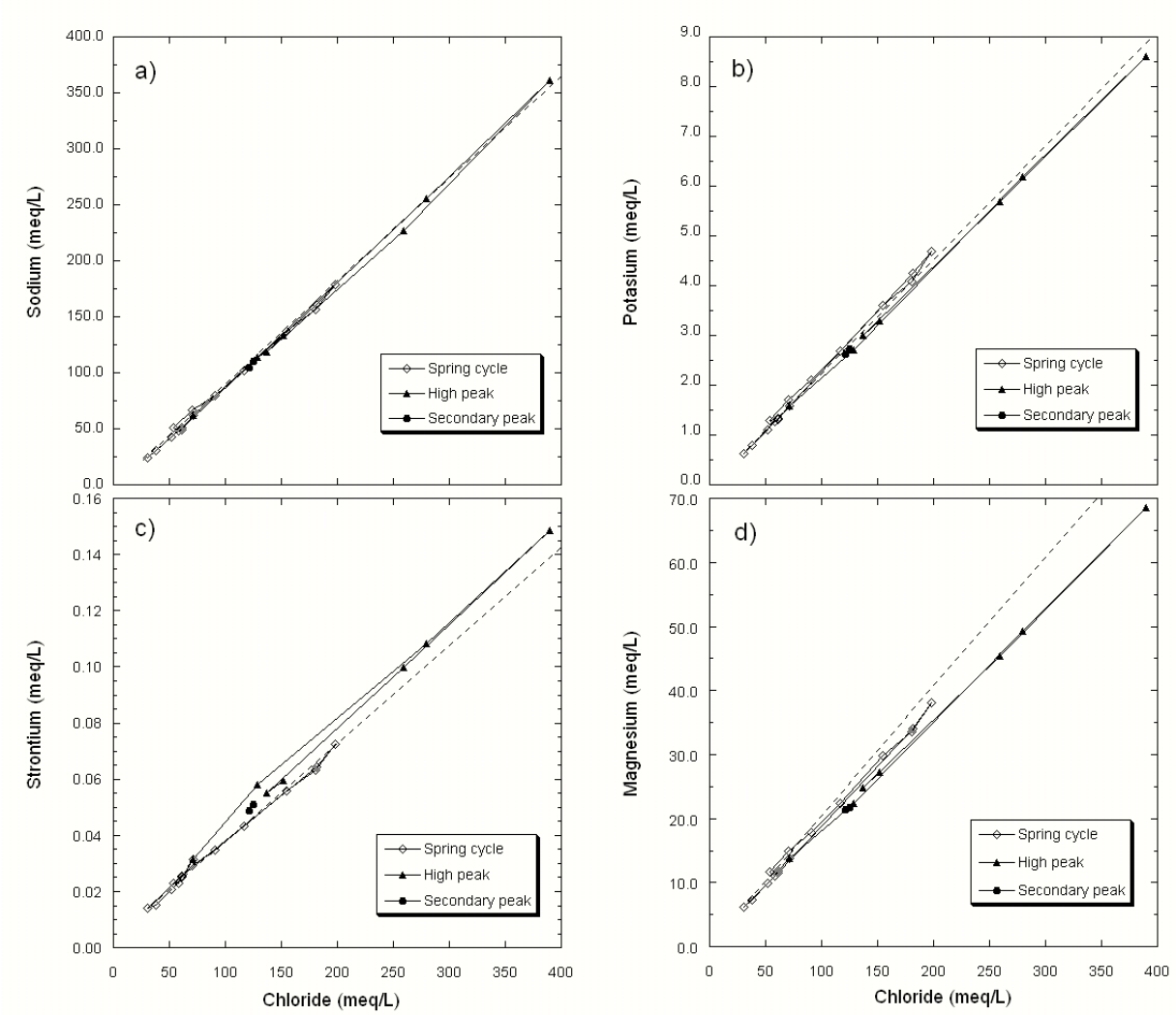

Figure 4.4: Relationship of major ions with the chloride content, for the sampling period of November-December 2004. Analyses are grouped as the spring stage they represent: spring cycle, high salinity peak after summer (high peak) and secondary salinity peak (secondary peak). Dashed line represents the conservative mixing between the fresher water sampled in the spring and the local seawater (M-21 and Local sea in Table 4.1, respectively).

4.1.3. Geochemical conceptual model for S'Almadrava spring

In Chapter 3 we proposed a dual-permeabilty hydraulic conceptual model of S'Almadrava spring (Figure 3.8) that explains both the main pattern of salinity variation and the formation of the double high salinity peak and secondary peaks. The model assumes that the mixed water moving up from the conduit branching is divided in two components: a fast turbulent flow occurring in a well developed fast conduit, and a low Darcyan flow through an intensely fissured matrix. The higher residence time in the matrix with respect to that of the open conduit enables to produce a delay in the arrival time of the high salinity mixed water to the spring mouth, that would explain the occurrence salinity peaks. The water discharging at the spring mouth comes

mainly from the karst conduit for high discharges but this proportion changes gradually as the total spring discharge decreases. That is, for low flows the proportion of fluid from the matrix on the total discharge increases.

Results in Figure 4.3 and Figure 4.4 show the differences on water chemistry during the high and secondary salinity peaks, and those during the spring cycle with respect to conservative mixing. Thus, the excess of Ca and Sr coexists with the depletion of K and Mg. Therefore, according to the cations behavior we postulate that cation-exchange may be one of the relevant processes of S'Almadrava spring. The Ca and Sr equivalent excess, however, is higher than the K and Mg depletion. This unbalance may be attributed to the difficulty to differentiate distinct patterns for Na results. Note that the relative much higher concentration of Na may prevent the recognition of a potential depletion of Na to fit the charge balance of a potential multi-ion exchange reaction.

The ionic exchange processes are known to be relatively frequent in karst coastal aquifers, whenever exchangers are present (Appelo et al., 1990, Beekman, 1991, Fidelibus et al., 2005). In the case of S'Almadrava spring, clay minerals have been identified in deep cores drilled in the vicinity of the spring outlet. Several clay core samples from the Raethian and lower Lias were analyzed by XRD giving 10-30% of Illite and up to 20% of Montmorillonite. Therefore, some ion exchange would be likely to occur.

The exchange between Ca^{2+} and Na^{+} is the most common reaction occurring in coastal aquifers. Thus, if a Ca-rich clay comes in contact with a solution in which Na^{+} is the dominant cation, the solution enriches in Ca^{2+} and loses Na^{+}, until the attainment of a new equilibrium. Thus, for example, this process may produce the increase in Ca during the high and secondary salinity peaks. The opposite reaction should also occur, that is, during the refreshing process when a new rainfall event is produced would turn the solid composition to its original composition, thus modifying the quality of the solution (e.g., releasing Na^{+} to solution and removing Ca^{2+}). But the ion-exchange reactions may also affect to the other main ions in solution, in our case K^{+}, Mg^{2+} and Sr^{2+}, according to their relative preference to enter the exchanger sites. Thus, the extent of the exchange turns out to be a quite complex process in flow systems and has to be modeled together with flow.

In the conceptual model proposed for S'Almadrava spring, the potential exchanger is located in the fissured matrix because (1) it presents low flow rates that would avoid the erosion of clay materials (as it may happen in the karst conduit), (2) it presents a low solid:solution ratio that would favor the ion-exchange reactions to occur at greater extent, and (3) the proportion of fluid from the fissured matrix is higher during the high and secondary salinity peak, consistently with the situations at which cation deviation from conservative mixing was observed.

In addition to the ion-exchange reactions, dissolution/precipitation of calcite due to the mixing waters is also likely to occur. When these processes are overlapped, the geochemical system

becomes even more difficult since, for example, the increase of Ca concentration due to calcite dissolution will promote further exchange of Ca with the rest of cations. This could be another explanation for the Ca excess in the equivalent balance, and will be discussed later.

4.2. Numerical modeling

4.2.1. Model settings

The simulation of this complex geochemical conceptual model can only be addressed by means of reactive transport modeling methods. The field data of spring flow discharge field during the sampling period was used as an input to the dual permeability model presented in Chapter 3 (TURBOCODE). The simulation was then optimized for reproducing the salinity measurements on Figure 4.1. The conceptual flow model used is in Figure 4.5 a conduit of freshwater connecting with the aquifer further inland, a conduit of seawater connected to the sea, and a conduit and a fissured matrix connecting conduit the branching with the spring mouth. The parameters in Table 4.2 were obtained after calibration with the salinity evolution trend for the sampling period of 2004 (Figure 4.6). The similarity of the calibrated parameter values with respect to the calibration obtained in Chapter 3 for an annual period in 1996, reveals the robustness of the numerical simulation and the stability of the spring functioning along the years.

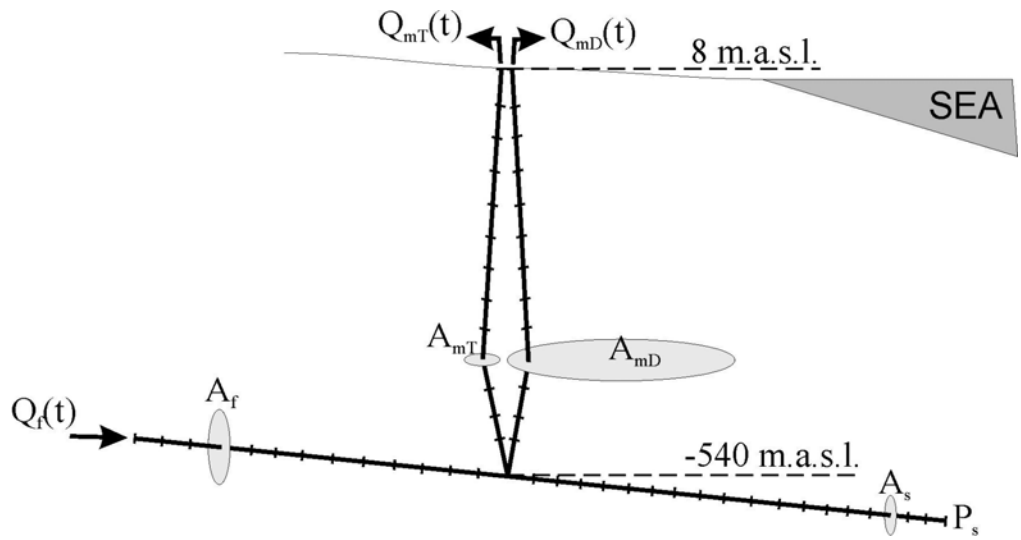

Figure 4.5: Scheme of the 2D mesh with 1D elements used for the reactive transport simulation of S'Almadrava spring. Boundary conditions are also indicated. Ovals represent the relative sections of the elements in every conduit (not scaled).

The flow distribution among the two permeable media (open karst conduit and fissured matrix) resulting from the calibrated hydraulic simulation was an input a reactive transport solver, RETRASO (Saaltink et al. 2004). The code RETRASO (Reactive TRAnsport of Solutes)

simulates reactive transport of dissolved and gaseous species in non-isothermal saturated or unsaturated problems. The code has been used in a wide range of problems, involving the solution of reactions of complexation, sorption, precipitation-dissolution of minerals and gas dissolution. The numerical simulation with RETRASO consists on a 2D mesh with 1D elements representing the four conduits operating in the system (Figure 4.5). The size and properties of the different conduits are set the same that those of the hydraulic simulation with TURBOCODE. Flow boundary conditions are time dependent functions of freshwater entering the system ($Q_f(t)$) and mixed water flowing out the system through the karst conduit ($Q_{mT}(t)$) and the fissured matrix ($Q_{mD}(t)$). The boundary condition at the opening of the seawater conduit to the sea bottom is a constant pressure, allowing the seawater input to maintain the mass balance in the system. The chemistry of the boundary freshwater was obtained from the fresher water sampled in the spring and that of the seawater from the local seawater sampled at the Pollença Bay (M-21 and Local sea in Table 4.1, respectively). A pCO_2 of 1.8 for the freshwater was calculated assuming equilibrium with calcite while maintaining Ca concentration and the pH measured in the field. It is not possible to estimate the pH and pCO_2 for the seawater at depth. We assume a pCO_2 value of 1.9 to ensure the equilibrium with calcite for the measured pH and Ca concentration. This value is close to measurements in deep wells found for a similar seawater intrusion setting (Ng and Jones, 1995). It should be noted the high sensitivity of the simulation results in terms of potential for calcite dissolution with the pCO_2 of the end-member solutions or the mixing place. This issue will be addressed in detail in Chapters 5 and 6.

The initial condition of concentration in the system was obtained from a preliminary simulation of a series of spring cycles until a steady behaviour is obtained. Ion exchange is allowed only in the fissured matrix and the conduit branching. A Cation Exchange Capacity of 15 meq/100 g of solid, was obtained as the best fit for the cation/Cl ratios (see a sensitivity analysis below). The cation exchange coefficients for K^+, Ca^{2+}, Mg^{2+} and Sr^{2+} with respect to Na^+ were obtained from Appelo and Postma (2005). Since exchange reaction take place in a few hours, we have assumed this process in equilibrium)

The kinetic dissolution of calcite is allowed in the entire system with a dissolution rate according to the expression of. The dissolution rate, r, follows the expression

$$r = \sigma k(\Omega - 1) \qquad (4.1)$$

where σ is the reactive area, k is the dissolution coefficient (Arvidson et al. 2003), and Ω is the saturation. A reactive surface area of 10 m^2/m^3_{rock} equivalent to a cylinder of 0.4 m of diameter was assumed for the fast conduit. A higher reactive surface of 50 m^2/m^3_{rock} was assumed for the matrix conduit. The sensitivity of the results with respect to the reactive surface area will be discussed below.

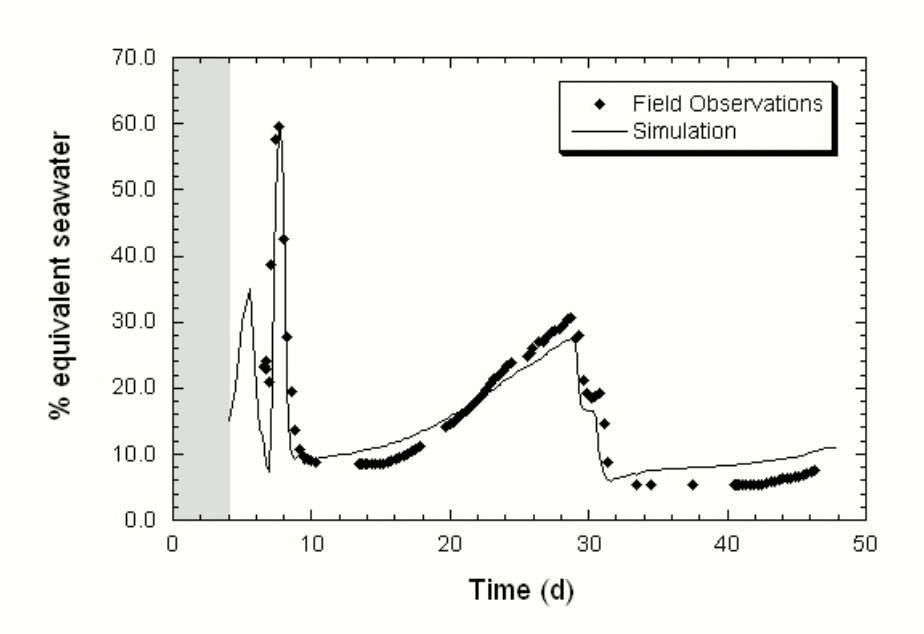

Figure 4.6: Comparison of field observations with the simulation results for the dual permeability reactive transport model for S'Almadrava spring, during the sampling period of 2004. Salinity is expressed in terms of % of equivalent seawater. Grey area shows the period when the spring is dry.

Table 4.2: List of optimal parameter values used for calibration of S'Almadrava spring discharge during the sampling period of 2004, using a dual permeability model. The meaning of the parameters is explained in Chapter 3.

Parameter	Value
L_s	4000.0 m
A_s	0.30 m^2
n_s	2.0×10^{-2}
z_B	-540.0 m.a.s.l.
n_{mT}	1.5×10^{-2}
A_{mT}	1.0 m^2
k_{mD}	0.5×10^{-6} m^2
A_{mD}	120.0 m^2
A_f	20.0 m^2

4.2.2. Results and discussion

Cation relationships

Results of the reactive transport calculation are shown in Figure 4.7 and Figure 4.8 in terms of relations of concentration of the cations with respect to Chloride. Results correspond to the sampling period on 2004 and therefore can be compared with the field data on Figure 4.3 and Figure 4.4. It should be noted that the simulation allow us to predict qualitatively the variation of the discharge composition during the double high salinity peaks after the summer. Prediction and experimental results are not plotted together to simplify the figures. The simulation results also show two main tendencies for every cation described for the field data observations: one for the high and secondary salinity peaks and secondary salinity peak, and another one for the spring cycle between consecutive rainfall events. The ion exchange generates an increase in the concentration of Ca^{2+} and Sr^{2+} in solution and a depletion of K^{+}, while the model has no appreciable effect on the concentration of Na^{+}. The simulation also shows that although the Na^{+} is actually being incorporated to the exchange complex replacing the Ca^{2+} and Sr^{2+}, the difference with respect the conservative mixing is not appreciable due to its higher concentration in solution. The refreshing of the exchangeable solid by freshwater is produced in a very short time period immediately after a new rainfall event is produces. This is observed as a very few calculated points in Figure 4.7 and Figure 4.8. This indicates the need for a very intense sampling frequency during this period.

It is important to recognize that the behaviour of Mg^{2+} does not follow the patterns observed in the field observations. In fact, it tends to slightly increase its concentration in solution during the salinitzation process, contrary to clear depletion observed in the field observations. This disagreement may due to the lack of information regarding exchange coefficients (average values from literature were used in the calculation). Dolomitization, another potential sink for Mg, is not likely to occur at this media owing to the high velocity of the water in the system. The model reproduces the qualitatively pattern observed in the field observations, thus suggesting the validation of the dual permeability conceptual model for S'Almadrava spring.

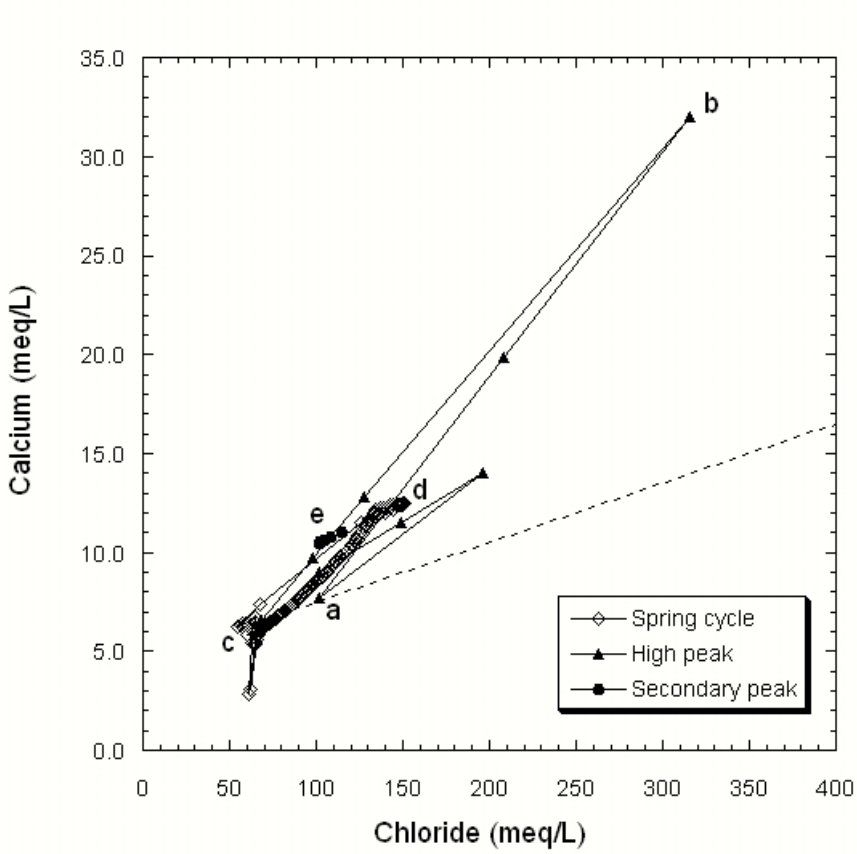

Figure 4.7: Relationship of Ca with chloride content as resulting from the reactive transport simulation, during the sampling period of November-December 2004. Dashed line represents the conservative mixing between end-member solutions in the simulation. Letters indicate particular stages of the spring discussed in the text.

As shown in Figure 4.7 and Figure 4.8 another interesting output from calculations is that the effect of the exchange processes can be observed not only during the high and secondary salinity peaks but also at the periods of low discharge (spring cycle). Therefore, unlikely to what it could be deduced from the experimental trend, the composition of the discharge during this period also differs from that of a pure mixing model (see deviation with respect to the dashed line in Figure 4.7). This feature was only observed in some experimental points with high Cl concentration (near point d in Figure 4.3 and Figure 4.7).

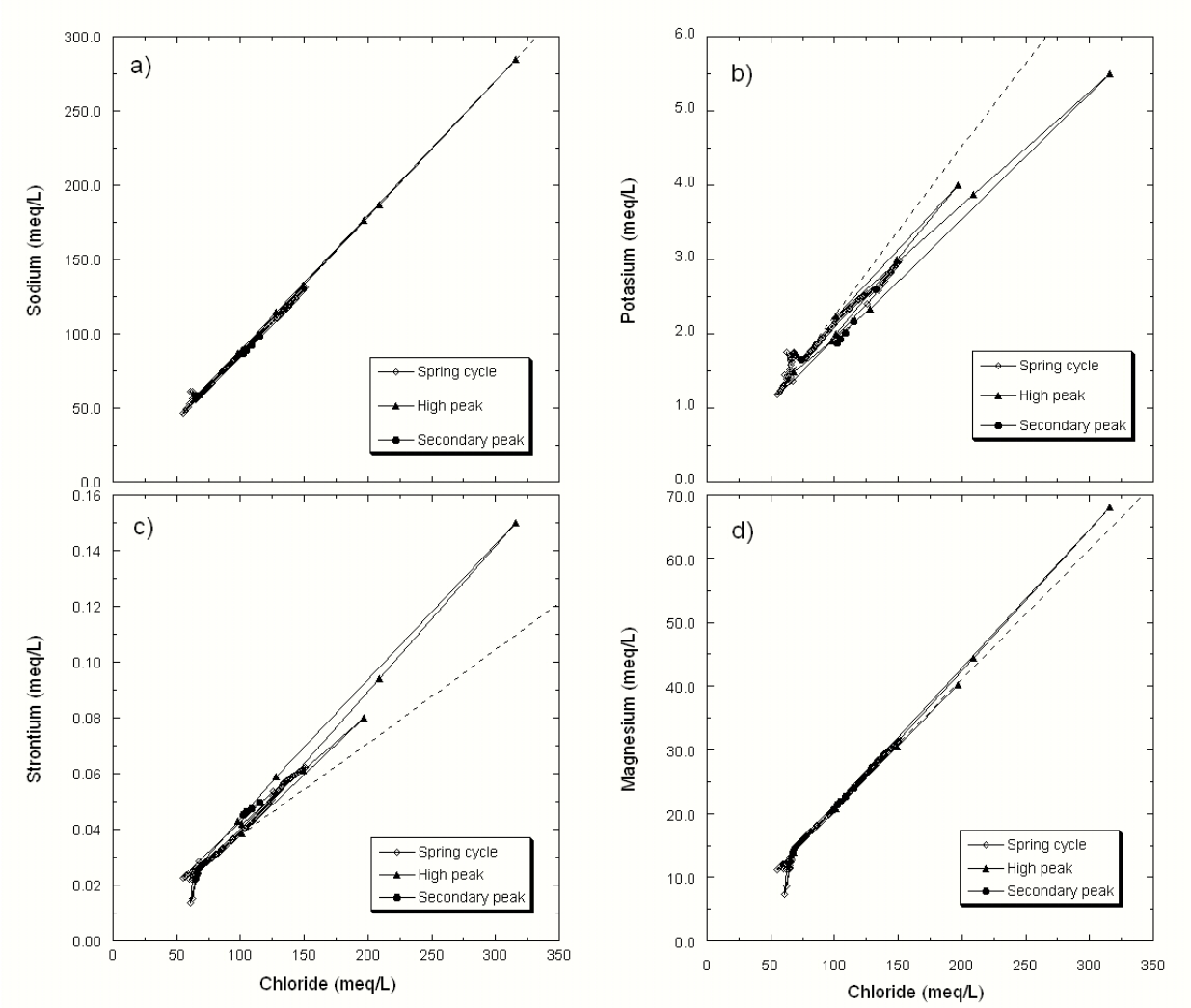

Figure 4.8: Relationship of major ions Na, K, Sr and Mg with chloride content as resulting from the reactive transport simulation, during the sampling period of November-December 2004. Dashed line represents the conservative mixing between end-member solutions in the simulation.

Calcite dissolution

The reactive transport simulation allows predicting the distribution of calcite dissolution and the porosity generated. As discussed before, these results can only be discussed qualitatively, since the total calcite dissolved will strongly depend on the pCO_2 of the end-member solutions considered for the simulation. During one spring cycle, the dissolution of calcite is likely to occur on the conduit branching (where the mixing waters occurs) and on the ascending conduits leading to the spring mouth. Figure 4.9 shows the spatial distribution of calcite dissolved in the karst conduit and the fissured matrix. Results are the integrated dissolution/precipitation of calcite along one representative spring cycle to facilitate the understanding. Because of the mixing of waters is undersaturated in calcite (recall that the end-members are assumed to be equilibrated with calcite), the maximum dissolution is obtained at -540 m, the depth of the conduit branching, where the mixing is produced (Figure 4.9). It should be noted that at this depth, the estimated dissolved calcite is the same for both the fast conduit and matrix since they

reach the conduit branching at the same location. Further, the high flows occurring at the conduit branching prevent dissolution to reach equilibrium. For the fast conduit, dissolution of calcite is predicted along the entire conduit because the very fast flows occurring in this conduit prevent calcite equilibrium to be reached. Dissolution decreases upwards as the water approaches to equilibrium.

The calcite dissolution predicted for the fissured matrix is more complex. Contrary to what happened in the karst conduit, dissolution of calcite does not occur in the entire length of the matrix media and becomes negligible above -400 m.a.s.l., approximately (Figure 4.9). This situation is due to the lower flow occurring at the matrix that allows the dissolution to progress to near equilibrium. At some point the mixed water flowing upwards saturates in calcite and stops dissolving. Calculations performed with reactive surfaces higher than 50 m^2/m^3_{rock} result in a similar pattern, with calcite equilibrium reached at deeper levels (not represented).

If ion-exchange processes are included, dissolution of calcite continues to occur up to the spring mouth. This is so because the ion-exchange reactions consume Ca and maintain the subsaturation in calcite in the pathway, thus favouring the dissolution of calcite. Thus, during the refreshing period when a new rainfall event occurs, the Na occupying exchanger is replaced by the Ca in solution, thus increasing the subsaturation of the mixed water with respect to calcite. It is important to note that during the salinization period between rainfall events the inverse exchange reaction occurs, Ca is removed by Na from the exchange complex and calcite eventually precipitates. However, the temporal integration of the calcite dissolution/precipitation along an entire spring cycle leads to a net dissolution budget (Figure 4.9).

It is interesting to note that the accumulated dissolution in the fast conduit is much higher than that predicted for the fissure matrix. This is due to the much larger flow occurring through the fast conduit. This pattern leads to a better development of the fast conduit along its entire length, increasing the hydraulic differences between the fast conduit and the matrix with time.

The results of the calculations also evidence that the effect of calcite dissolution/precipitation from the ion concentration of the spring discharge is practically undistinguishable (results not shown). The ion-exchange processes occurring in S'Almadrava spring would overlap the effects of calcite dissolution/precipitation. This result can be one of the reasons for the contradictory observations on calcite dissolution found in freshwater-seawater mixing zones around the world and discussed in Chapters 5 and 6.

Sensitivity to the Cation Exchange Capacity

The sensitivity of the simulation with respect to the Cation Exchange Capacity (CEC) used in the simulations is also explored because of the high uncertainty of this parameter in the model. Results obtained for three values of CECare shown in Figure 4.10. Increasing the CEC value enhances the extent of the ion exchange processes of both salinization and refreshing. Thus,

the deviation of the composition of the spring discharge with respect to the pure mixing of freshwater and seawater increases with the CEC value used. In other words, reducing the CEC of the fissured matrix leads to composition variation resulting from a pure mixing of the two end-members of the system. The high sensitivity of the results to this parameter value allowed us to precise the limits of the potential range of CEC values of the underground lithology.

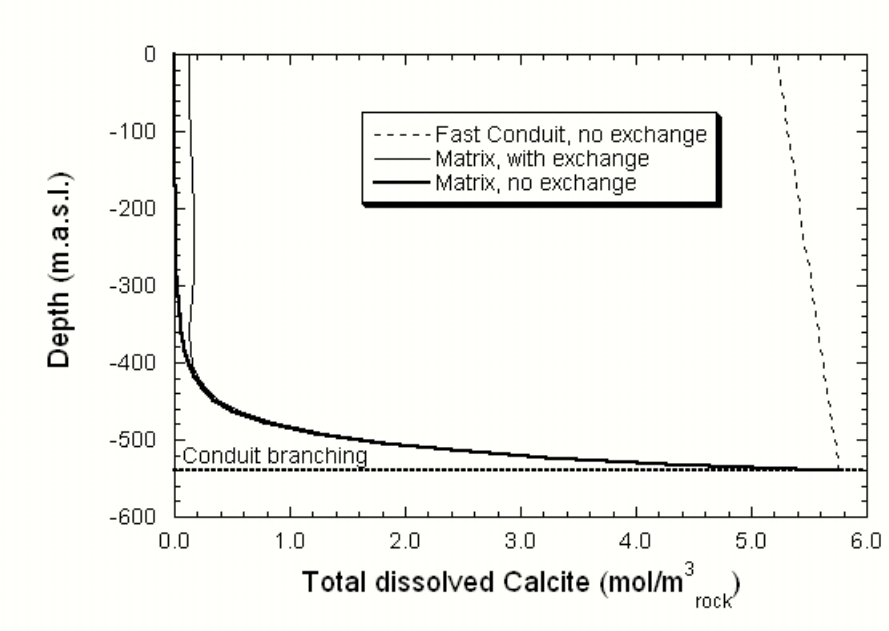

Figure 4.9: Distribution of accumulated calcite dissolution during only one representative spring cycle in the fast flow karst conduit and the low flow fissured matrix, for S'Almadrava spring. Results correspond to reactive transport simulations in which the effect of considering ion-exchange in the fissured matrix is also explored. The horizontal dashed line indicates the position of the conduit branching.

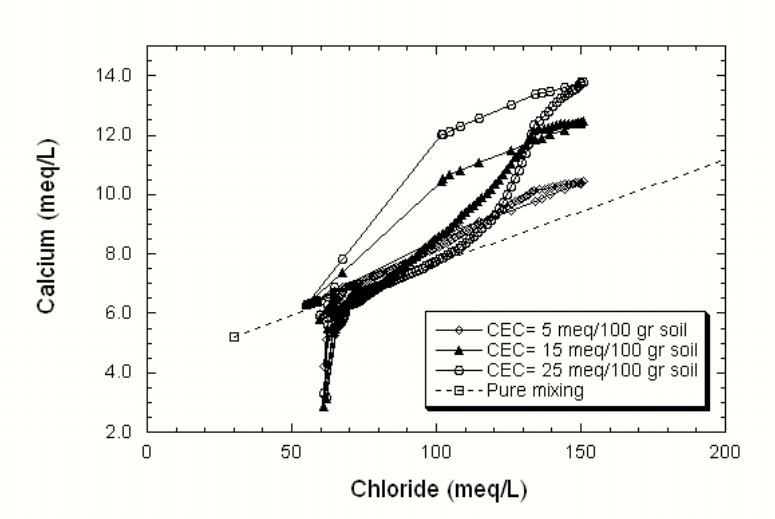

Figure 4.10: Sensitivity of the relationship of calcium and chloride concentrations with the Cation Exchange Capacity (CEC) used in the simulation. Results correspond to one spring cycle between consecutive rainfall events. Dashed line represents the conservative mixing between the end-member solutions used in the simulation (M-21 and Local sea, in Table 4.1).

4.3. Conclusions

The dual permeability hydraulic conceptual model proposed for S'Almadrava spring in Chapter 3 was coupled to water-rock interactions to explain the geochemical signature of the spring discharge obtained after a high frequency sampling campaign after the long dry summer of 2004. The flow field was first obtained using the TURBOCODE solver (Chapter 3) and then use as input for the RETRASO code to simulate reactive transport. Reactive transport modeling is the ones way to interpret chemical data in such a dynamic and complex system. The availability of detailed geochemical data allows the identification of ion exchange processes as the dominant of the system, with an increase of Ca^{2+} and Sr^{2+} concentration, and a reduction of K^{+} and Mg^{2+} during the salinization exchange, and vice versa for the refreshing. Results obtained with the reactive transport calculations reproduce major ions/chlorite values, in terms of relationships of the patterns observed in the field observations. The exception of Mg is attributed to the lack of information of exchange coefficients for the exchange complexes working on the area of the study. The model also allow to calculate the Cation Exchange Capacity of the fissured matrix to reasonable values based on the deviation of the major ions with respect to the composition observed during the spring cycle.

Simulations predict that calcite dissolution is occurring in the system for the end-member solutions selected. For the end-member solutions used in this study, calcite dissolution and porosity development is predicted to occur mainly at the conduit branching but also along both the fast flow and low flow conduits leading to the spring mouth. The porosity development appears to be very sensitive to dissolution rate considered. The solution for the fissured matrix resulted especially interesting since the dissolution/precipitation of calcite appears influenced by the ion exchange processes occurring in the system. Thus, during the salinization process, Ca^{2+} is released from the solid promoting an oversaturation (and further precipitation) of calcite in solution. On the contrary, during the refreshing process, the Ca^{2+} is depleted from the solution to exchange with the Na^{+} in the solid, and the subsaturation of the solution with respect to calcite increases. The dissolution produced during the low salinity periods is more important than the precipitation during the high salinity discharges and the net result is the creation of porosity.

Dissolution of calcite is not recognizable from the composition of the spring discharge neither on the field measurements nor on the simulation results. However, this result is a bit disappointing since it prevents from the identification of calcite dissolution at depth, from the chemistry of the discharge of brackish springs.

The satisfactory performance of the simulation reproducing the field observations allow to further validate the dual permeability conceptual model for S'Almadrava spring. This conclusion reveals the importance of applying techniques to complement the purely hydraulic studies to

further validate the conceptual models proposed for brackish springs. High frequency geochemical data appears to be a powerful tool for this purpose.